Robotica (2013) volume 31, pp. 361–369. © Cambridge University Press 2012
doi:10.1017/S0263574712000343

Learning to swim: a dynamical systems approach to mimicking fish swimming with CPG

Tianmiao Wang†, Yonghui Hu‡* and Jianhong Liang†

†*School of Mechanical Engineering and Automation, Beihang University, Beijing 100191, P. R. China*
‡*School of Control and Computer Engineering, North China Electric Power University, Beijing 102206, P. R. China*

(Accepted June 21, 2012. First published online: July 18, 2012)

SUMMARY
Central Pattern Generators (CPGs) can generate robust, smooth and coordinated oscillatory signals for locomotion control of robots with multiple degrees of freedom, but the tuning of CPG parameters for a desired locomotor pattern constitutes a tremendously difficult task. This paper addresses this problem for the generation of fish-like swimming gaits with an adaptive CPG network on a multi-joint robotic fish. Our approach converts the related CPG parameters into dynamical systems that evolve as part of the CPG network dynamics. To reproduce the bodily motion of swimming fish, we use the joint angles calculated with the trajectory approximation method as teaching signals for the CPG network, which are modeled as a chain of coupled Hopf oscillators. A novel coupling scheme is proposed to eliminate the influence of afferent signals on the amplitude of the oscillator. The learning rules of intrinsic frequency, coupling weight and amplitude are formulated with phase space representation of the oscillators. The frequency, amplitudes and phase relations of the teaching signals can be encoded by the CPG network with adaptation mechanisms. Since the Hopf oscillator exhibits limit cycle behavior, the learned locomotor pattern is stable against perturbations. Moreover, due to nonlinear characteristics of the CPG model, modification of the target travelling body wave can be carried out in a smooth way. Numerical experiments are conducted to validate the effectiveness of the proposed learning rules.

KEYWORDS: Biomimetic robotic fish; Central pattern generator; Fish swimming kinematics; Dynamical systems; Learning.

1. Introduction

The astonishing swimming capabilities of aquatic animals (e.g., fish and cetaceans) have attracted substantial research interests in bio-mechanisms of swimming and building of biorobotic underwater vehicles in the last decade.[1,2] The hydrodynamic interaction between the swimming organisms and the fluid environment constitutes a quite complex problem for biologists and engineers, while artificial devices of biological propulsion and maneuvering hold great promises to achieve higher efficiency, greater maneuverability and lower noise radiation than conventional screw-propelled vehicles. With the increasing understanding of the swimming mechanisms of aquatic animals and the progress in material, sensor, control and fabrication, the nautical technology that we have been acquainted with will be revolutionized in the future.

Recent years have seen the emergence of a variety of swimming machines that mimic the morphology and locomotion of fish, with research emphasis ranging from experimental investigation and validation of fish hydrodynamics,[3,4] modeling and control theoretic analysis,[5–7] engineering demonstration and field deployment,[8,9] to education and exhibition.[10–12] A fundamental problem that needs to be solved for robotic fish is how to control the movement of tail in order to generate thrust forces effectively. An instinctive approach is to reproduce the empirically observed bodily motion of swimming fish with multiple tail linkages connected by rotating joints.[13,14] Although accurate mimicry of fish movements can be obtained with such a trajectory approximation method, it requires time-consuming numerical computations that are unsuitable for real-time control, and online modification of the target kinematic model is difficult to be realized. In refs. [15] and [16], a sine-based approach that applies phase-lagging sinusoidal signals to the serially connected joints is employed to generate propulsive travelling waves. The explicit relationship between joint kinematics and the governing sine equation allows easy adjustment of the amplitude, frequency and wavelength of the swimming motion. However, online modification of the parameters of the sine function will cause discontinuous jump of joint angles which might damage the actuator and the transmission mechanisms. An important concept from neurophysiology which has been extensively used for locomotion control of robots is Central Pattern Generator (CPG).[17,18] It has been generally accepted that many rhythmic movements in locomotion, such as walking, running, swimming and flying, are controlled by CPG neural circuits that are found in both vertebrate and invertebrate animals. CPG can produce coordinated oscillatory signals in the absence of sensory inputs or descending inputs from higher cognitive elements. A few studies have examined the biologically inspired swimming control of robotic fish utilizing CPG.[19–25] The CPG-based method allows easy implementation and online generation of the swimming gait. The intrinsic nonlinear characteristics of CPG enables smooth transitions between gaits, as well as adaptations to both perturbations of state variables and modifications of

* Corresponding author. E-mail: huyhui@gmail.com

the control parameters. However, there is not yet a well-established design methodology that can be used to achieve a particular desired locomotion behavior for a particular robot structure. The determination of CPG model type, coupling topology and sensory feedback pathways are based mostly on experience, and much effort is required to tune the CPG parameters by hand or by an optimization algorithm.

In this paper, we investigate the problem of mimicking the bodily motion of swimming fish with a chain of adaptive CPGs for an articulated robotic fish. The objective is to combine the advantages of both the trajectory approximation method and the CPG-based method. Rhythmic movements of the tail joints are driven by the outputs of CPGs, which are modeled mathematically as a network of coupled nonlinear oscillators. Learning rules which provide adaptation mechanisms are proposed to dynamically tune the parameters of the oscillators and the coupling strengths between them, according to the kinematic model of swimming fish. After learning, CPG outputs with appropriate frequency, amplitudes and phase relations can be acquired, thus the instructed locomotor pattern can be reproduced by the robotic fish. The proposed learning method provides a synthesis tool for the CPG-based control, and meanwhile guarantees the biological basis for generation of swimming gaits on the robotic fish.

The paper is organized as follows. Section 2 presents the derivation of teaching signals from fish kinematics, the CPG model with input transformation and the learning rules to acquire the instructed locomotor pattern with CPG. In Section 3, we demonstrate the effectiveness of the proposed method by numerical simulations. Conclusions are drawn and future works are discussed in Section 4.

2. Learning Fish Swimming with CPG

In this section, we first derive teaching signals for CPG from the swimming kinematics of fish, then the CPG model employed for joint angle control of the robotic fish is presented and finally the learning rules that enable reproduction of the instructed swimming gait are proposed.

2.1. Deriving teaching signals from fish swimming kinematics

Majority of fish species use body/caudal fin (BCF) undulations for propulsion. Carangiform is the most common BCF swimming style in nature, and fish utilizing carangiform swimming exhibits remarkable performance in both speed and efficiency.[1] For carangiform swimmers, the body undulations are restricted to the rear third of the body, and the forward part of the body remains relatively immobile. For application of fish swimming on underwater vehicle system, carangiform swimming mode bears the advantages of high speed, high efficiency and easy implementation. Consequently, most studies of robotic fish have focused on carangiform swimming, which also serves as the kinematic model for learning fish-like swimming in this study.

Biological observations have shown that the kinematics of carangiform swimmers is generally in the form of a backward travelling wave with the amplitude increasing from the nose to the tail. Lighthill[26] suggested a specific form of travelling wave that describes the body-spline of a swimming fish:

$$y_{\text{body}}(x,t) = (c_1 x + c_2 x^2) sin(kx - \omega t), \tag{1}$$

where $y_{\text{body}}(x,t)$ represents the transverse displacement of the fish body, x denotes the displacement along the body axis, $k = 2\pi/\lambda$ indicates the body wave number, λ is the body wave length, c_1 is the linear wave amplitude envelope, c_2 is the quadratic wave amplitude envelope, $\omega = 2\pi f$ is the body wave frequency (in rad s^{-1}), f is the body oscillation frequency and t is the time. Equation (1) specifies a sinusoidal wave that propagates from the fish's center of mass to the tail bounded by a second-order amplitude envelope.

Given the swimming kinematics of fish, the following task is to reproduce the bodily motion on robotic fish with limited number of tail joints. In refs. [13] and [14], a link-based body wave fitting technique is proposed to numerically fit the spatial- and time-varying body wave at discrete time instants with a planar, serial chain of links connected with oscillating joints. The end-point coordinates $(x_{i,j}, y_{i,j})$ of the ith link at the jth instant of a swimming cycle can be obtained from the following equation:

$$\begin{cases} (x_{i,j} - x_{i-1,j})^2 + (y_{i,j} - y_{i-1,j})^2 = l_i^2 \\ y_{i,j} = (c_1 x_{i,j} + c_2 x_{i,j}^2) sin(k x_{i,j} - \frac{2\pi j}{M}) \end{cases}, \tag{2}$$

where $i = 1, \ldots, N$, N denotes the number of links, $j = 1, \ldots, M-1$, M is the number of discrete instants in a swimming cycle and l_i represents the length of the ith link. With the end-point coordinates of each link, the joint angles can thus be calculated iteratively as

$$\theta_{i,j} = arctan \frac{y_{i+1,j} - y_{i,j}}{x_{i+1,j} - x_{i,j}} - \theta_{i-1,j}, \tag{3}$$

where $\theta_{i,j}$ denotes the angle of the ith joint at instant j. Figure 1 shows a schematic illustration of the trajectory approximation method for a four-link robotic fish. The variations of joint angles calculated with this method are shown in Fig. 2. The joints oscillate in a nearly sinusoidal manner, with the same frequency, different amplitudes and specific phase shifts. In Section 2.3, the joint angles obtained with the trajectory approximation method will be used as teaching signals for a network of CPGs. The waveform of

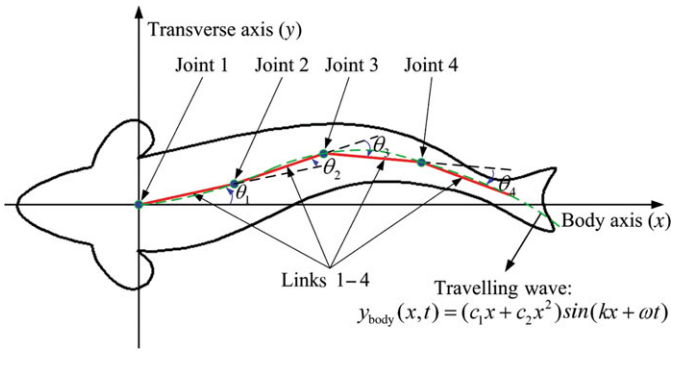

Fig. 1. (Colour online) Schematic illustration of the trajectory approximation method.

https://doi.org/10.1017/S0263574712000343 Published online by Cambridge University Press

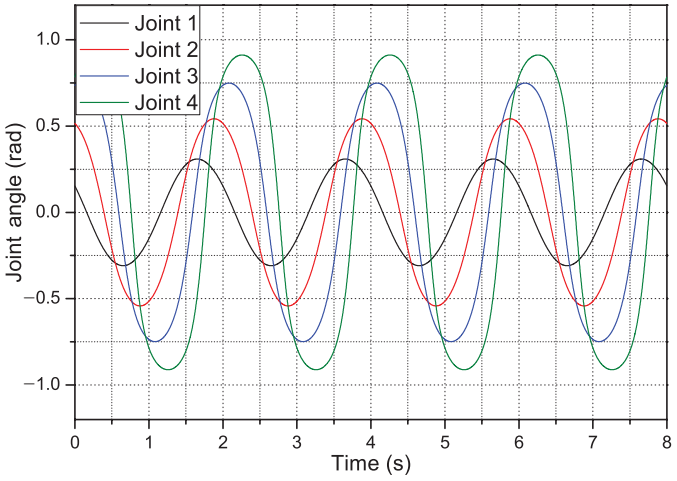

Fig. 2. (Colour online) The joint angles calculated with the trajectory approximation method. The body wave is given by $y_{\text{body}}(x,t) = (0.2x + 0.5x^2)sin(2x - \pi t)$, and the lengths of all the links are set as 0.25.

the CPG's oscillatory outputs and the phase relations between them will be learned, so that the swimming kinematics of fish can be reproduced when driving the joints with the CPG outputs.

2.2. CPG model for generation of swimming gait

Ichthyology studies reveal that rhythmic patterns of neural activity exist in the axial motion of fish body. The swimming movements generated by waves of left–right alternating motor activity that travel rostrocaudally along the body are considered to be controlled by spinal CPGs.[27] Therefore, we employ a network of coupled CPGs to generate rhythmic swimming movements on the robotic fish.

The CPG model that we utilize is based on the Hopf oscillator. The dynamics of the oscillator is governed by the following nonlinear differential equations:

$$\begin{cases} \dot{u} = (\rho - r^2)u - \omega v \\ \dot{v} = (\rho - r^2)v + \omega u \end{cases}, \tag{4}$$

where $r = \sqrt{u^2 + v^2}$, u and v are state variables in Cartesian space, $\rho > 0$ controls the amplitude of the oscillation and ω specifies the intrinsic frequency of the oscillator (in rad s^{-1}). The Hopf oscillator has a harmonic limit cycle, and the steady state solution of the system can be written as $u_\infty(t) = \sqrt{\rho}cos(\omega t + \phi_0)$ and $v_\infty(t) = \sqrt{\rho}sin(\omega t + \phi_0)$, where ϕ_0 is determined by the initial condition. The analytical solution of the oscillator facilitates parameter specification for a desired oscillation behavior. Further, the limit cycle is structurally stable, which means small perturbations on the oscillator do not change the general behavior of the system and once the perturbation is gone, it will converge back to its original trajectory.

Each joint of the robotic fish is allocated with a CPG, and the target angle of the joint is determined by the CPG output, which equals the state variable u of the Hopf oscillator. To generate fish-like swimming patterns, oscillations of the joints should be coordinated by connecting them together with appropriate coupling scheme. The coupling term is most often implemented as an additive perturbation on the nonlinear oscillator. The general form of additive perturbation can be represented by the following equations:

$$\begin{cases} \dot{u} = (\rho - r^2)u - \omega v + p_u \\ \dot{v} = (\rho - r^2)v + \omega u + p_v \end{cases}, \tag{5}$$

where p_u and p_v are the components of the perturbation acting on u and v state variables, respectively. The perturbation signal can influence the phase dynamics of the oscillator, thus inter-joint coordination can be achieved in such a way that one oscillator perturbs another in order to realize frequency synchronization and to maintain a stable phase difference between them.

However, the oscillation amplitude of the perturbed oscillator will also be modified, which is an undesirable side effect of the perturbation. To illustrate how the perturbation signal influences the amplitude and phase dynamics of the oscillator, we rewrite the perturbed oscillator equation in polar coordinates. By setting $u = rcos\phi$ and $v = rsin\phi$, Eq. (5) can be transformed into

$$\begin{cases} \dot{r} = (\rho - r^2)r + p_u cos\phi + p_v sin\phi \\ \dot{\phi} = \omega - \frac{p_u}{r} sin\phi + \frac{p_v}{r} cos\phi \end{cases}. \tag{6}$$

It can be seen from Eq. (6) that there is no equilibrium point of the amplitude due to the complex influence of the perturbation, which makes it hard to specify parameter for a desired oscillation amplitude. To eliminate this influence, components of the perturbation signal are required to satisfy the following relationship: $p_u cos\phi + p_v sin\phi = 0$. For an afferent signal p, we allow some kind of input transformations $p_u(\cdot)$ and $p_v(\cdot)$ before it acts on the state variables of the oscillator, so that the above relationship can be satisfied. A viable form of transformations can be represented by the following equations:

$$\begin{cases} p_u(p) = \frac{pv^2}{r} \\ p_v(p) = -\frac{puv}{r} \end{cases}. \tag{7}$$

The oscillator perturbed by signal p with the above input transformations can thus be described in polar coordinates as

$$\begin{cases} \dot{r} = (\rho - r^2)r \\ \dot{\phi} = \omega - psin\phi \end{cases}. \tag{8}$$

It is obvious from the equation that the amplitude remains unperturbed and only the phase is affected. The entrainment property of the nonlinear oscillator can be reserved after transformation of the periodic input signal. Figure 3 shows the structure of the CPG model based on the Hopf oscillator with input transformation.

The phase relations among a network of CPGs can be achieved by feeding weighted states u and v of one oscillator

https://doi.org/10.1017/S0263574712000343 Published online by Cambridge University Press

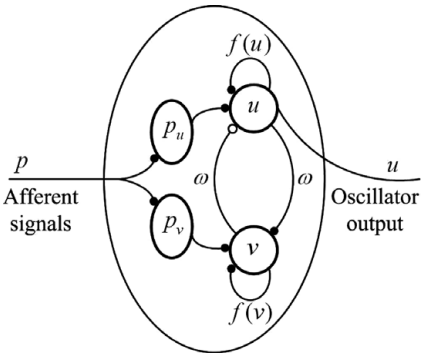

Fig. 3. CPG model based on Hopf oscillator with input transformation.

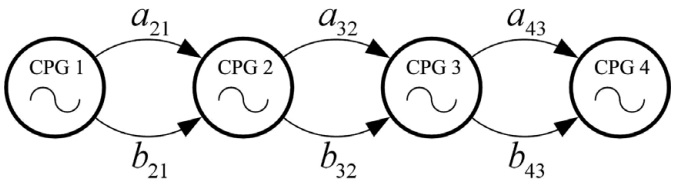

Fig. 4. CPG network implemented to generate fish-like swimming gait.

to the other, as illustrated by the following equations:

$$\begin{cases} \dot{u}_i = (\rho_i - r_i^2)u_i - \omega_i v_i + \sum_j \dfrac{(a_{i,j}u_j + b_{i,j}v_j)v_i^2}{r_i} \\ \dot{v}_i = (\rho_i - r_i^2)v_i + \omega_i u_i - \sum_j \dfrac{(a_{i,j}u_j + b_{i,j}v_j)u_i v_i}{r_i} \end{cases}, \tag{9}$$

where $a_{i,j}$ and $b_{i,j}$ denote the connection weights between the ith and the jth oscillator. The phase difference between the coupled oscillators is determined by the connecting weights $a_{i,j}$ and $b_{i,j}$.

The CPG network is constructed as a chain of Hopf oscillators, following the tail structure of the robotic fish. For simplicity, only neighboring oscillators are connected. Both unidirectional and bidirectional couplings can induce phase synchronization between oscillators. But less parameters that need to be tuned are required for unidirectional coupling. Thus, only descending couplings are assumed, which follows that each oscillator can only be affected by its adjoining frontal oscillator. With this setting, the coupling weights $a_{i,j}$ and $b_{i,j}$ that do not satisfy $i = j + 1$ will be set as zero. Figure 4 shows the structure of the CPG network implemented to generate the fish-like swimming gait.

2.3. Learning rules for CPG

The waveform of the teaching signal obtained numerically from the kinematics of swimming fish is almost sinusoidal, therefore it can be approximated by the harmonic output of the Hopf oscillator with appropriate frequency and amplitude. The phase relations between the teaching signals should also be learned in order to generate the propulsive travelling wave. An optimization and search algorithm is feasible to find the suitable CPG parameters for reproduction of the instructed locomotor pattern. But heavy computational cost is generally required. In this study, we propose a dynamical systems approach to the acquisition of an appropriate parameter set. By converting the parameters controlling frequency, phase difference and amplitude into new state variables with their own dynamics, the waveforms of the teaching signals and their phase relations can be encoded by the CPG network in a simple and efficient way. The learning is embedded into the dynamics of the oscillator, and no external optimization or preprocessing of the teaching signal is required.

During learning, the teaching signal for each CPG is received by the oscillator as an additive perturbation. Then the network of CPG, with coupling between adjacent oscillators and additive inputs of the periodic teaching signals, can be described by the following equations:

$$\begin{cases} \dot{u}_i = (\rho_i - r_i^2)u_i - \omega_i v_i + \dfrac{a_{i,i-1}u_{i-1}v_i^2}{r_i} \\ \quad + \dfrac{b_{i,i-1}v_{i-1}v_i^2}{r_i} + \dfrac{\varepsilon T_i v_i^2}{r_i} \\ \dot{v}_i = (\rho_i - r_i^2)v_i + \omega_i u_i - \dfrac{a_{i,i-1}u_{i-1}u_i v_i}{r_i} \\ \quad - \dfrac{b_{i,i-1}v_{i-1}u_i v_i}{r_i} - \dfrac{\varepsilon T_i u_i v_i}{r_i} \end{cases}, \tag{10}$$

where T_i is the teaching signal for the ith oscillator, and $\varepsilon > 0$ is an adaptation constant. By transforming equation (10) into polar coordinates, we obtain:

$$\begin{cases} \dot{r}_i = (\rho_i - r_i^2)r_i \\ \dot{\phi}_i = \omega_i - a_{i,i-1}r_{i-1}cos\phi_{i-1}sin\phi_i \\ \quad -b_{i,i-1}r_{i-1}sin\phi_{i-1}sin\phi_i - \varepsilon T_i sin\phi_i \end{cases}. \tag{11}$$

The phase space representation shows clearly how the behavior of the limit cycle system is influenced by external perturbations. In the following, we derive the learning rules of frequency, coupling weight and amplitude from a geometric point of view.

2.3.1. Learning frequency. In this paper, since the teaching signals are derived from Eq. (1) that explicitly specifies the body wave frequency, we can directly assign the value of body wave frequency to the intrinsic frequency of the Hopf oscillator, avoiding the need for an adaptation mechanism. However, when the teaching signals are obtained in other ways, the learning of frequency may become necessary. For example, we can record the swimming motion of live fish and use the trajectories of some marked points on fish body as the teaching signals. In that case, the frequency is not given explicitly and has to be learnt from the recorded data. Therefore, we present the learning rules for frequency that enables frequency adaptation to instructed locomotor behavior in a more general form.

The frequency of a periodically driven self-sustained oscillator will change toward the frequency of the input signal. When the frequency mismatch between the oscillator and the input signal is small, the oscillator gets entrained, i.e., it oscillates at the frequency of the input signal.[28] But this frequency adaptation is only temporary. Once the

https://doi.org/10.1017/S0263574712000343 Published online by Cambridge University Press

input signal is removed, the oscillator immediately returns to its intrinsic dynamics. In order to enlarge the range of frequencies in which synchronization occurs and to maintain the learned frequency after the external driving signal disappears, dynamic plasticity is developed for the oscillator in refs. [29] and [30], in the sense that the parameter controlling the intrinsic frequency of the oscillator is allowed to change dynamically.[29,30] The adaptation mechanism, called the Dynamic Hebbian learning, is developed according to the effects of external perturbation on the activity of the oscillator. In phase plane representation, a periodic perturbation can result in an average acceleration or deceleration of the rotating phase point. This effect can be used to tune the intrinsic frequency of the oscillator. An ordinary differential equation, with the intrinsic frequency as the state variable and the effect of perturbation on phase dynamics as the evolving law, drives the intrinsic frequency of the oscillator toward the frequency of the perturbation. The convergence properties of the adaptive frequency oscillator are presented in ref. [29].

We design the frequency adaptation mechanism for the Hopf oscillator with input transformation following the approach presented in refs. [29] and [30]. The influence of external perturbation on phase dynamics of oscillator is shown in Eq. (11). Thus, the adaptation law for learning the frequency of the teaching signal is given by the following equation:

$$\dot{\omega}_i = -a_{i,i-1} r_{i-1} cos\phi_{i-1} sin\phi_i - b_{i,i-1} r_{i-1} sin\phi_{i-1} sin\phi_i - \varepsilon T_i sin\phi_i. \quad (12)$$

The intrinsic frequency changes according to the total effect of the input signals. It is apparent that the input signals contain only one frequency component, namely the common frequency of the teaching signals for the joints. Therefore, after learning all the joints will oscillate at the frequency of the instructed propulsive wave.

2.3.2. Learning coupling weight. The coupling from one oscillator to another is to maintain correct phase difference between them, so that the phase relations will not be destroyed by external perturbations after learning. As has been discussed above, the coupling between a pair of oscillators is a composite signal coming from the two state variables of the forcing oscillator, each alone producing some phase lag on the forced oscillator. By adjusting the relative strengths of components of the signal, a range of phase difference between oscillators can be attained.

The input signal can influence the instantaneous frequency of the forced oscillator, and accelerates or decelerates the phase point depending on the input signal and the state of the oscillator (i.e., the position of the point on the limit cycle). To evaluate how much the phase point is pushed forward or pulled back by the input signal within a given time interval, we can integrate the perturbation term acting on the phase of the oscillator over that time interval. We formulate the learning algorithm of coupling weights by using the time-averaged effects of the input signals on phase dynamics of the oscillator. With the correlation-based learning rule, the coupling weight should be enforced when the signal from the forcing oscillator and the teaching signal push the phase point in the same direction, and be weakened otherwise. The learning rule that modulates the coupling weights to produce the phase difference specified by the teaching signals takes the following form:

$$\dot{a}_{i,i-1} = \gamma \int_{t-\tau_i}^{t} r_{i-1} cos\phi_{i-1} sin\phi_i dt \int_{t-\tau_i}^{t} T_i sin\phi_i dt, \quad (13)$$

$$\dot{b}_{i,i-1} = \gamma \int_{t-\tau_i}^{t} r_{i-1} sin\phi_{i-1} sin\phi_i dt \int_{t-\tau_i}^{t} T_i sin\phi_i dt, \quad (14)$$

where γ is a positive constant controlling the learning rate, and $\tau_i = 2\pi/\omega_i$ is the oscillation period of the ith oscillator, indicating that the time-averaged effects are evaluated over an oscillatory cycle of the oscillator.

2.3.3. Learning amplitude. When an oscillator is perturbed by an external periodic signal with frequency equal to its intrinsic frequency, it can achieve in-phase synchronization with the input signal, i.e., the phase difference between them settles to zero.[28] With the frequency adaptation mechanism, the intrinsic frequency of the CPG converges to the frequency of the input signal, so that the timing of the CPG output will become in-phase with the input signal. In the CPG network, the phase dynamics of an oscillator is influenced not only by the teaching signal but also by signals from its adjacent oscillator. The learning rule of coupling weights ensures that the composite signal from the forcing oscillator and the teaching signal can be tuned to synchronize with zero phase difference, which implies in-phase synchronization between the CPG output and the teaching signal.

With the proposed input transformation of afferent signals, the amplitude of the oscillator is solely determined by the parameter ρ, which can also be converted into a state variable with its own evolving dynamics. The learning rule is based on the correlation between the CPG output and its difference with the teaching signal, which is given by the following equation:

$$\dot{\rho}_i = \eta(T_i - r_i cos\phi_i) r_i cos\phi_i, \quad (15)$$

where η is a positive constant that determines the rate of learning. The adaptation of amplitude starts when the CPG output and the teaching signal become in-phase. The evolution law increases the amplitude when the CPG output and the error signal are correlated, and decreases the amplitude when uncorrelated. The amplitude converges to the maximum value of the teaching signal, in which case the waveform of the CPG output matches the waveform of the teaching signal.

In Section 2.2, we presented a network of Hopf oscillators for reproduction of fish swimming gait. The learning rules of intrinsic frequency, coupling weight and amplitude for the CPG network are formulated in polar coordinates in Section 2.3. By transforming the learning rules into Cartesian coordinates and combining the rules with the CPG model, we obtain an adaptive CPG network with six state variables,

https://doi.org/10.1017/S0263574712000343 Published online by Cambridge University Press

which are described by the following equations:

$$\begin{cases} \dot{u}_i = (\rho_i - r_i^2)u_i - \omega_i v_i + \dfrac{a_{i,i-1}u_{i-1}v_i^2}{r_i} \\ \quad + \dfrac{b_{i,i-1}v_{i-1}v_i^2}{r_i} + \dfrac{\varepsilon T_i v_i^2}{r_i} \\ \dot{v}_i = (\rho_i - r_i^2)v_i + \omega_i u_i - \dfrac{a_{i,i-1}u_{i-1}u_i v_i}{r_i} \\ \quad - \dfrac{b_{i,i-1}v_{i-1}u_i v_i}{r_i} - \dfrac{\varepsilon T_i u_i v_i}{r_i} \\ \dot{\omega}_i = -\dfrac{a_{i,i-1}u_{i-1}v_i}{r_i} - \dfrac{b_{i,i-1}v_{i-1}v_i}{r_i} - \dfrac{\varepsilon T_i v_i}{r_i} \\ \dot{a}_{i,i-1} = \gamma \displaystyle\int_{t-\tau_i}^{t} \frac{u_{i-1}v_i}{r_i}dt \int_{t-\tau_i}^{t} \frac{T_i v_i}{r_i}dt \\ \dot{b}_{i,i-1} = \gamma \displaystyle\int_{t-\tau_i}^{t} \frac{v_{i-1}v_i}{r_i}dt \int_{t-\tau_i}^{t} \frac{T_i v_i}{r_i}dt \\ \dot{\rho}_i = \eta(T_i - u_i)u_i \end{cases} . \quad (16)$$

3. Numerical Simulations

In this section, we conduct numerical experiments with the adaptive CPG to show the effectiveness of the proposed learning rules.

3.1. Learning sinusoidal signals

To examine the learning ability of the adaptive CPG network, we first use sinusoidal signals that can be described explicitly as the teaching signals. Since the CPG network used to mimic fish swimming has unidirectional coupling and only adjacent units are connected, it suffices to consider a pair of oscillators with couplings from one to the other. The sinusoidal teaching signals are described by the following equations:

$$T_1(t) = 1.2sin(2t - 0.2), \quad (17)$$

$$T_2(t) = 1.6sin(2t - 1.2). \quad (18)$$

The waveforms of the teaching signals and the CPG outputs at the beginning of learning and after learning are plotted in Fig. 5. Figure 6 shows the evolution of intrinsic frequency, coupling weight and amplitude. As shown in the figures, the second oscillator, which has a small frequency difference with the teaching signal at the beginning, quickly synchronizes with the teaching signal, whereas no frequency locking occurs to the first oscillator due to its large frequency difference with the teaching signal. With the proposed learning rule, the intrinsic frequencies of both oscillators gradually adapt to the frequency of the teaching signals. But the intrinsic frequencies oscillate around rather than converge to the desired frequency. The amplitudes of the oscillations are determined by the learning rate. Therefore, the faster the oscillator learns, the larger will be the adaptation error. To attain the correct frequency of the teaching signal, we employ a first-order low-pass filter $\tau_f \dot{\overline{\omega}} = -\overline{\omega} + \omega$ to attenuate the oscillation, where τ_f is a time constant. When the learning stops, $\overline{\omega}$ is used as the intrinsic frequency of the oscillator.

The convergence values of coupling weights are determined not only by the phase difference between oscillators but also by their initial values and the initial phase difference. We investigate the evolution of coupling weights

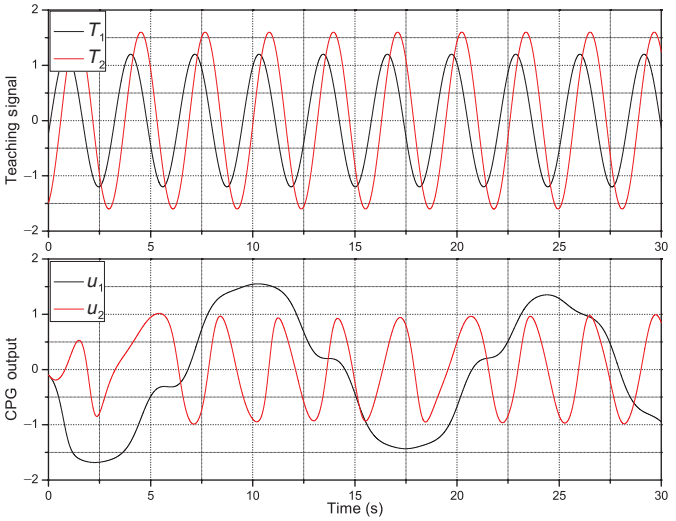

(a)

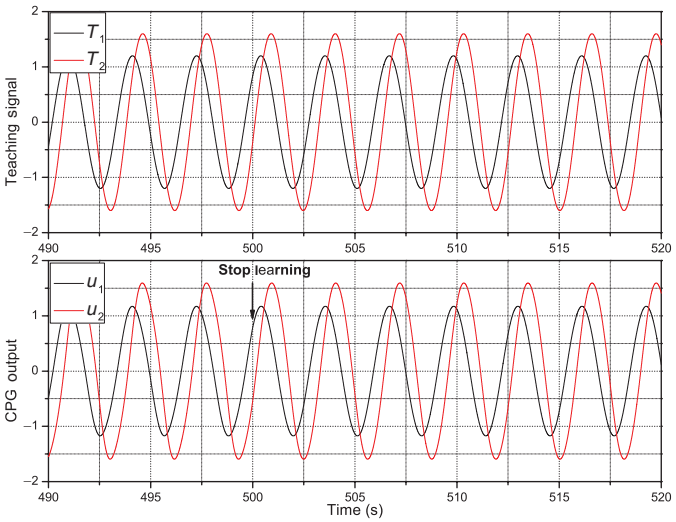

(b)

Fig. 5. (Colour online) The waveforms of the teaching signals and the CPG outputs at the beginning of learning and after learning. The arrow indicates the time to stop learning. The initial conditions are $\omega_1(0) = 0.5$, $\omega_2(0) = 3.0$, $\rho_1(0) = 3.0$, $\rho_2(0) = 1.0$, $a_{21}(0) = 0.6$ and $b_{21}(0) = 0.2$. The learning rates are $\varepsilon = 0.3$, $\gamma = 0.03$ and $\eta = 0.04$. The convergence values of the parameters are shown in Fig. 6. (a) At the beginning of learning. (b) After learning.

with several pairs of initial values and the same initial phase difference. Table I shows the initial and convergence values of coupling weights, with the phase difference specified by Eqs. (17) and (18). It illustrates that different combinations of coupling weights can produce the same phase difference. But the ratios of a_{21} and b_{21} are almost the same, which follows that the relative strength of coupling weights is what really matters to the phase difference. Hence, if we fix one of the coupling weights to some nonzero value and allow the other to evolve, appropriate combination of coupling weights can also be attained. In addition, the dependence of convergence values of coupling weights on initial phase difference between oscillators is examined. As shown in Table II, with the same initial values of coupling weights

https://doi.org/10.1017/S0263574712000343 Published online by Cambridge University Press

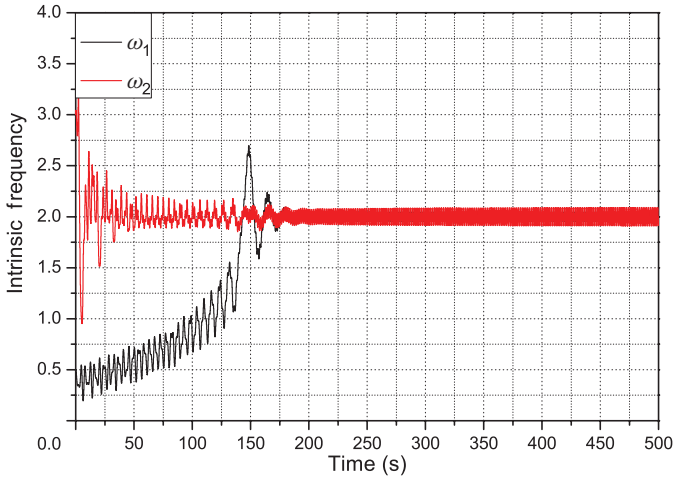

(a)

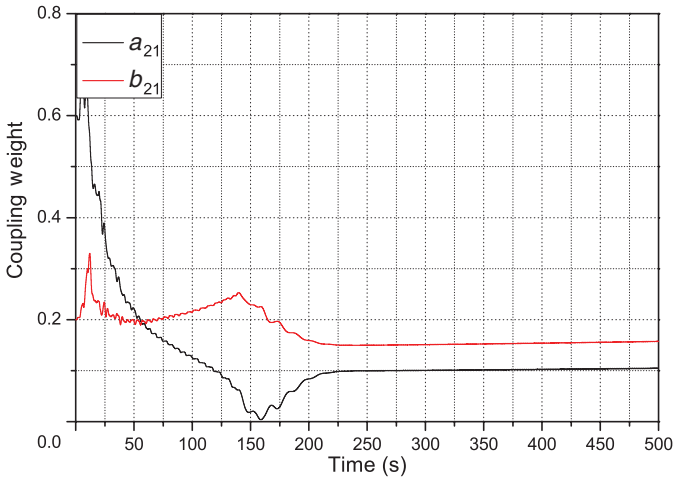

(b)

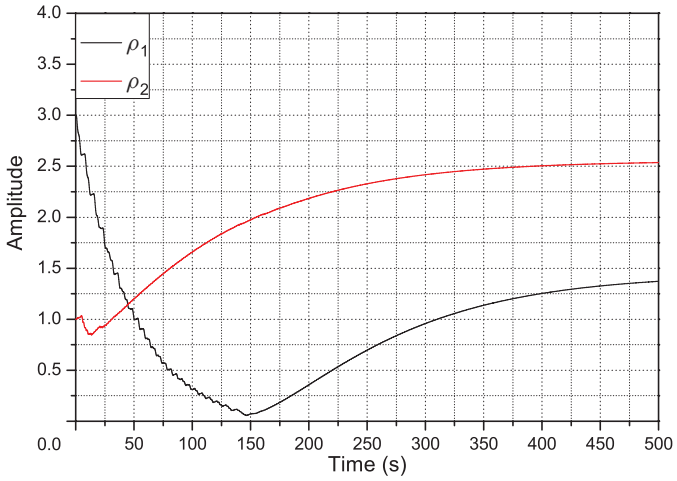

(c)

Fig. 6. (Colour online) The evolution of intrinsic frequency, coupling weight and amplitude during learning. (a) The evolution of intrinsic frequency. (b) The evolution of coupling weight. (c) The evolution of amplitude.

and different initial phase differences, several combinations of coupling weights are obtained, while their relative strength remains almost fixed.

To validate the correctness of the coupling weights, we perturb one of theoscillators to change the phase difference between them with transient perturbation. As shown in Fig. 7, a transient perturbation is superimposed on the state variable of the second oscillator at some random time after learning, and as a result the phase difference is changed. But after a short transition period, the phase difference recovers its earlier value before perturbed. It is obvious that the phase relation has been correctly encoded by the coupling weights.

Before the oscillator and its teaching signal become in-phase, the amplitude decreases quickly. To avoid negative value of the amplitude that will cause failure of the learning, small learning rate should be used. Once in-phase synchronization is achieved, the amplitude starts to adapt to the desired value.

Table I. Convergence values of coupling weights with different initial values and the same initial phase difference.

Initial values		Convergence values		Ratio of convergence values
a_{21}	b_{21}	a_{21}	b_{21}	
0.6	0.2	0.104645	0.157384	0.664902
0.8	0.05	0.096500	0.145116	0.664985
0.2	0.04	0.065210	0.098047	0.665089
0.2	0.1	0.089655	0.134821	0.664993
0.1	0.1	0.062226	0.093560	0.665092
0.05	0.1	0.040589	0.073151	0.665022
0.01	0.15	0.068786	0.103429	0.665055
0.04	0.16	0.084315	0.126782	0.665039

Table II. Convergence values of coupling weights with the same initial values and different initial phase difference. Note that the initial phase difference is determined by the initial values of state variables. The initial coupling weights are $a_{21} = 0.1$ and $b_{21} = 0.1$.

Initial values of state variables				Convergence values		Ratio of convergence values
u_1	v_1	u_2	v_2	a_{21}	b_{21}	
−0.1	0.1	−0.1	0.1	0.062226	0.093560	0.665092
−0.1	0.1	0.1	−0.1	0.089473	0.134544	0.665009
−0.1	0.1	−0.1	−0.1	0.109308	0.164408	0.664858
−0.1	0.1	0.1	0.1	0.109779	0.165133	0.664791

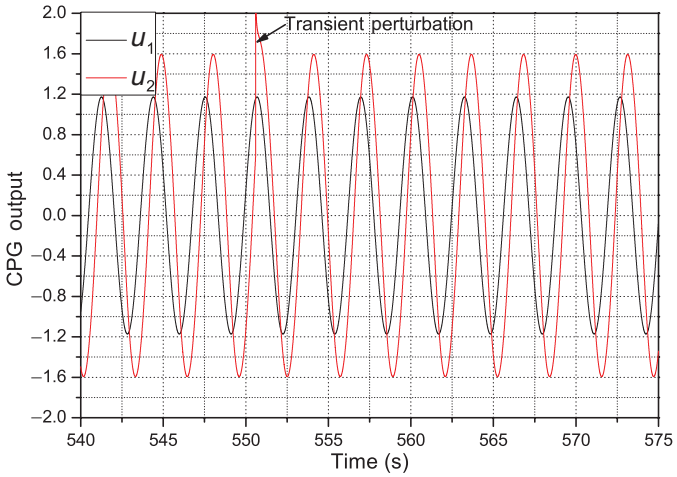

Fig. 7. (Colour online) The response of the oscillator to transient perturbation.

https://doi.org/10.1017/S0263574712000343 Published online by Cambridge University Press

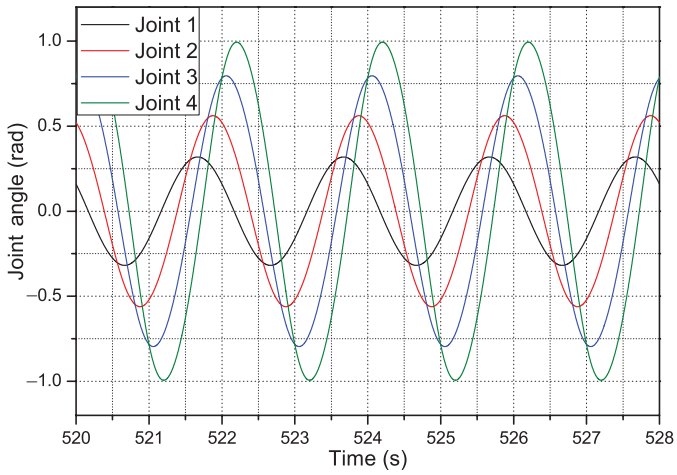

Fig. 8. (Colour online) The joint angles generated by the CPG network after learning. The convergence values of the parameters are as follows: $\omega_1 = \omega_2 = \omega_3 = \omega_4 = 3.1416$, $\rho_1 = 0.0916$, $\rho_2 = 0.3050$, $\rho_3 = 0.6233$, $\rho_4 = 0.9769$, $a_{21} = 0.4410$, $b_{21} = 0.3483$, $a_{32} = 0.4692$, $b_{32} = 0.2967$, $a_{43} = 0.5163$, $b_{43} = 0.2397$.

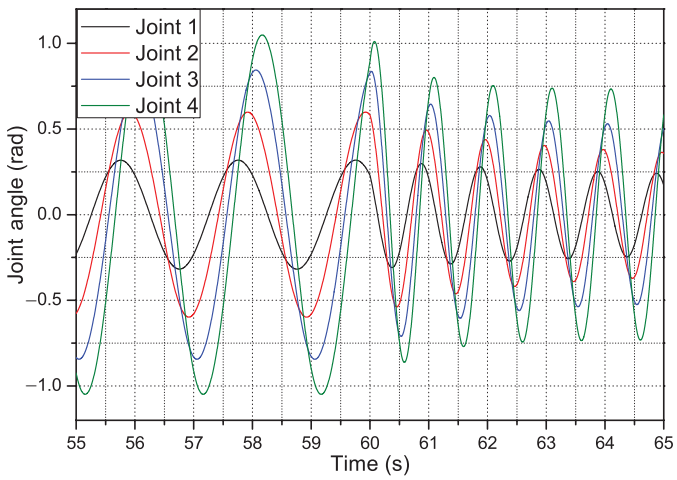

Fig. 9. (Colour online) The joint angles generated by the CPG network when the travelling wave is changed. The body wave is given by $y_{\text{body}}(x, t) = (0.2x + 0.5x^2)sin(2x - \pi t)$ before $t = 60$, and $y_{\text{body}}(x, t) = (0.1x + 0.15x^2)sin(4x - 2\pi t)$ after $t = 60$.

In conclusion, with appropriate learning rates, the adaptive CPG network can learn frequency, coupling weight and amplitude of sinusoidal teaching signals in a single stage. The intrinsic frequency and amplitudes learned by the proposed method ensure that the CPG outputs and the teaching signals will overlap, and the coupling weights guarantee the stability of phase relations between oscillators.

3.2. Learning fish swimming gaits

To learn fish swimming gaits with the CPG network, we use the joint angles $\theta_{i,j}$ calculated with the trajectory approximation method as the teaching signals. In numerical simulations, the teaching signals are discrete in time, so that we have $T_i(j) = \theta_{i,j}$, where $i = 1, \ldots, 4$ and j is the discrete time number. Figure 8 shows the joint angles generated by the CPG network after learning. Compared with the teaching signals shown in Fig. 2, the desired frequency, amplitudes and phase relations are obtained. Although there exist small adaptation errors with the amplitudes, which are caused by the non-sinusoidal waveforms of the teaching signals, the effectiveness of the proposed learning rules can be validated.

Learning of the desired travelling body waves can be carried out offline on a computer. Once the appropriate CPG parameters are obtained, the differential equations describing the CPG model are integrated numerically with the microcontroller onboard the robotic fish to generate the swimming gait online. Change of the travelling wave can be achieved through modification of the CPG parameters. Figure 9 shows the joint angles generated by the CPG network when the travelling wave is changed. The CPGs can adapt to abrupt parameter changes and converge to the new limit cycles quickly due to the nonlinear characteristics of the CPG model. The smooth transitions between different swimming gaits avoid jerky changes of the joint angles that may damage servomotors.

4. Conclusions and Future Works

In this contribution, we presented an adaptive CPG network capable of learning instructed locomotor pattern for a multi-joint robotic fish. To reproduce the bodily motion of a swimming fish, the joint angles calculated with the trajectory approximation method were used as the teaching signals. The CPG network was modeled as a chain of coupled Hopf oscillators. A novel coupling scheme is proposed to eliminate the influence of afferent signals on the amplitude of the oscillator. We formulated the learning rules of frequency, amplitude and coupling weight with phase plane representation of the oscillator. The effectiveness of the proposed learning rules was validated through numerical simulations.

The proposed learning method provides a novel approach to synthesizing CPG-based controllers that exhibit desired locomotor pattern. Compared with stochastic optimization methods, the instructed locomotor pattern can be encoded by the CPG network in an efficient and elegant way. The learning is embedded in the dynamical systems, as opposed to being implemented by an external algorithm. The main limitation of the method is that learning of frequency, phase relation and amplitude takes place serially, leading to slow convergence. The learning rates should be selected carefully in order to realize successful learning. In addition, the waveform of the teaching signals is limited to sinusoidal signals. In the future research, generalization of the method to other network topology than chain topology with unidirectional couplings, to other robot structures and teaching signals of other waveforms will be investigated. Sensory feedback will also be integrated to explore the dynamics of the neuromechanical system composed of neural oscillator, robotic fish and the fluid for high efficient swimming.

Acknowledgments

This work was supported by National Natural Science Foundation of China (Nos. 61105108, 61075100 and 51005008). The authors would like to thank the referees

https://doi.org/10.1017/S0263574712000343 Published online by Cambridge University Press

for careful reading of the manuscript and for their helpful comments.

References

1. M. Sfakiotakis, D. M. Lane and J. B. C. Davies, "Review of fish swimming modes for aquatic locomotion," *IEEE J. Ocean. Eng.* **24**, 237–252 (Apr. 1999).
2. P. R. Bandyopadhyay, "Trends in biorobotic autonomous undersea vehicles," *IEEE J. Ocean. Eng.* **30**(1), 109–139 (2005).
3. M. S. Triantafyllou and G. S. Triantafyllou, "An efficient swimming machine," *Sci. Amer.* **272**(3), 64–70 (1995).
4. G. Tan, G. Shen, S. Huang, W. Su and Y. Ke, "Investigation of flow mechanism of a robotic fish swimming by using flow visualization synchronized with hydrodynamic force measurement," *Exp. Fluids* **43**(5), 811–821 (2007).
5. Z. Chen, S. Shatara and X. Tan, "Modeling of biomimetic robotic fish propelled by an ionic polymer¤Cmetal composite caudal fin," *IEEE/ASME Trans. Mechatron.* **15**(3), 448–459 (2010).
6. K. A. Morgansen, B. I. Triplett and D. J. Klein, "Geometric methods for modeling and control of free-swimming fin-actuated underwater vehicles," *IEEE Trans. Robot.* **23**(6), 1184–1199 (2007).
7. Y. Hu, W. Zhao, G. Xie and L. Wang, "Development and target following of vision-based autonomous robotic fish," *Robotica* **27**, 1075–1089 (2009).
8. J. M. Anderson and P. A. Kerrebrock, "The Vorticity Control Unmanned Undersea Vehicle (VCUUV) – An Autonomous Vehicle Employing Fish Swimming Propulsion and Maneuvering," **In**: *Proceedings of the 10th International Symposia on Unmanned Untethered Submersible Technology* , Durham, NH (1997) pp. 189–195.
9. J. Liang, T. Wang and L. Wen, "Development of a two-joint robotic fish for real-world exploration," *J. Field Robot.* **28**(1), 70–79 (2011).
10. Y. Terada and I. Yamamoto, "An animatronic system including lifelike robotic fish," *Proc. IEEE* **92**(11), 1814–1820 (2004).
11. H. Hu, L. Liu, I. Dukes and G. Francis, "Design of 3D Swim Patterns for Autonomous Robotic Fish," **In**: *Proceedings of the IEEE/RSJ International Conference on Intelligent Robots and Systems* (2006) pp. 2406–2411.
12. J. Shao and L. Wang, "Platform for Cooperation of Multiple Robotic Fish – Robofish Water Polo," **In**: *Proceedings of the 46th IEEE Conference on Decision and Control* (2007) pp. 1423–1428.
13. J. Yu, M. Tan, S. Wang and E. Chen, "Development of a biomimetic robotic fish and its control algorithm," *IEEE Trans. Syst. Man Cybern. Part B Cybern.* **34**(4), 1798–1810 (2004).
14. J. Liu and H. Hu, "Biological inspiration: From carangiform fish to multi-joint robotic fish," *J. Bionic Eng.* **7**(1), 35–48 (2010).
15. K. Low and A. Willy, "Biomimetic motion planning of an undulating robotic fish fin," *J. Vib. Control* **12**(12), 1337–1359 (2006).
16. K. Hirata, "Development of Experimental Fish Robot," **In**: *Proceedings of the 6th International Symposia on Marine Engineering* (2007) pp. 711–714.
17. S. Grillner, "Neurobiological bases of rhythmic motor acts in vertebrates," *Science* **228**(4696), 143–149 (1985).
18. A. J. Ijspeert, "Central pattern generators for locomotion control in animals and robots: A review," *Neural Netw.* **21**(4), 642–653 (2008).
19. A. Crespi, D. Lachat, A. Pasquier and A. J. Ijspeert, "Controlling swimming and crawling in a fish robot using a central pattern generator," *Auton. Robot.* **25**(1–2), 3–13 (2008).
20. D. Zhang, D. Hu, L. Shen and H. Xie, "Design of an artificial bionic neural network to control fish-robot's locomotion," *Neurocomputing* **71**(4–6), 648–654 (2008).
21. W. Zhao, Y. Hu, L. Zhang and L. Wang, "Design and CPG-based control of biomimetic robotic fish," *IET Contr. Theory Appl.* 3(3), 281–293 (2009).
22. P. Arena, "A Mechatronic Lamprey Controlled by Analog Circuits," *Proceedings of the 9th IEEE Mediterranean Conference on Control and Automation*, Dubrovnik, Croatia (2001).
23. C. Zhou and K. H. Low, "Kinematic Modeling Framework for Biomimetic Undulatory Fin Motion Based on Coupled Nonlinear Oscillators," **In**: *Proceedings of the IEEE/RSJ International Conference on Intelligent Robots and Systems*, Taipei, Taiwan (2010) pp. 934–939.
24. L. Wang, S. Wang, Z. Cao, M. Tan, C. Zhou, H. Sang and Z. Shen, "Motion Control of a Robot Fish Based on CPG," **In**: *Proceedings of the IEEE International Conference Industrial Technology*, Hong Kong (2005) pp. 1263–1268.
25. M. Wang, J. Yu and M. Tan, "Modeling Neural Control of Robotic Fish with Pectoral Fins Using a CPG-Based Network," **In**: *Proceedings of the 46th IEEE Conference on Decision and Control* (2009) pp. 6502–6507.
26. M. J. Lighthill, "Note on the swimming of slender fish," *J. Fluid Mech.* **9**(3), 305–317 (1960).
27. F. A. Mussa-Ivaldi and S. A. Solla, "Neural primitives for motion control," *IEEE J. Oceanic Eng.* **29**(3), 660–673 (2004).
28. A. Pikovsky, M. Rosenblum and J. Kurths, *Synchronization, A Universal Concept in Nonlinear Sciences*, vol. 12 (Cambridge University Press, Cambridge, UK, 2001).
29. L. Righetti, J. Buchli and A. Ijspeert, "Dynamic hebbian learning in adaptive frequency oscillators," *Physica* D **216**(2), 269–281 (2006).
30. J. Buchli, F. Iida and A. J. Ijspeert, "Finding Resonance: Adaptive Frequency Oscillators for Dynamic Legged Locomotion," **In**: *Proceedings of the IEEE/RSJ International Conference on Intelligent Robots and Systems*, Beijing, China (2006) pp. 3903–3909.